Surface & Coatings Technology 392 (2020) 125756

Contents lists available at ScienceDirect

Surface & Coatings Technology

journal homepage: www.elsevier.com/locate/surfcoat

Duplex surface treatment of metallic alloys combining cold-spray and plasma electrolytic oxidation technologies

J. Martin[a,b,*], K. Akoda[a,b], V. Ntomprougkidis[a,b], O. Ferry[a], A. Maizeray[a,b,c], A. Bastien[c], P. Brenot[c], G. Ezo'o[c], G. Henrion[a,b]

[a] Université de Lorraine, CNRS, IJL, F-54000 Nancy, France
[b] Université de Lorraine, Laboratoire d'Excellence Design of Alloy Metals for low-mAss Structures ('LabEx DAMAS'), F-57045 Metz, France
[c] CRITT METALL 2/ICAR, Campus ARTEM, 2 allée André Guinier, 54000 Nancy, France

ARTICLE INFO

Keywords:
Duplex treatment
Cold-spray deposition
Plasma electrolytic oxidation (PEO)
Aluminium
Magnesium
Ferrous metals

ABSTRACT

Plasma electrolytic oxidation (PEO) is widely used to improve the corrosion and wear resistance of lightweight metals such as aluminium alloys by the formation of a ceramic oxide coating. However, the PEO process remains ineffective for ferrous metals and, when applied to magnesium alloys, oxide coatings are usually thin and porous. To overcome these limitations, the feasibility of applying a duplex treatment combining cold-spray deposition (CS) and PEO is investigated. Cold-sprayed aluminium coatings are deposited on magnesium (EV31) and steel (S235) substrates prior to PEO processing. Investigation of this duplex process evidences the efficiency of such a two-steps process to form thick, dense and crystalline alumina coatings on both magnesium and steel substrates. The growth kinetic of the duplex CS-PEO oxide layer is enhanced by a factor of 3 compared to single-step PEO processing of bulk aluminium substrates. Results are discussed by considering the effect of the porosity through the cold-sprayed aluminium coating on the mechanism of oxidation during the subsequent PEO treatment.

1. Introduction

Plasma electrolytic oxidation (PEO), also referred to as micro-arc oxidation (MAO), is a plasma-assisted electrochemical technology to synthesize protective ceramic-like oxide coatings on lightweight metals like aluminium, titanium and magnesium alloys [1–4]. PEO process is gaining a growing interest in various industrial domains (transport, energy, medicine) to replace conventional chromic acid anodizing (CAA) or hard acid anodizing (HAA) [5,6]. Indeed, PEO results in improved wear and corrosion resistance together with enhanced thermal stability and biocompatibility properties. The use of environmentally friendly alkaline electrolytes is an asset as well [6–8]. PEO process is carried out at a voltage slightly higher than the breakdown voltage of the growing oxide layer. Consequently, PEO coatings grow under a sparking regime leading to the gradual conversion of the processed metal to a crystalline oxide layer [9–12]. The growth mechanisms of the protective PEO coatings remain complex due to the combination of both electrochemical, thermal and plasma phase reactions that simultaneously occur in a small affected volume (few tens of μm^3) [13–17].

In the case of aluminium alloys, PEO process parameters are well controlled to form thick and compact oxide achieving a long-term protection. Numerous studies were devoted to the electrolyte composition according the requested coating properties [5,6,18]. Especially, the addition of (micro-) particles in the electrolyte aims at forming composite oxide layers (metal/oxide, oxide/oxide), that endows the protective layer with new functionalities [19–22]. In parallel, other studies sought the optimization of the electrical conditions, such as the applied supplying mode (AC, DC, bipolar, *etc.*), the current and/or voltage amplitude, or the frequency and duty cycle of the applied voltage or current [23–26]. Using a pulsed bipolar current to supply the electrodes promotes the appearance of a particular "soft" regime that occurs after a certain period of processing time [27–29] provided the current waveform parameters are suitably set. The occurrence of this "soft" regime is associated with the gradual decrease in the voltage response, the gradual disappearance of visible discharges as well as an increase in the growth rate and a lowering of the oxide coating porosity [30].

Although the PEO process of aluminium alloys is now well controlled, PEO processing of magnesium alloys faces some issues and PEO layers grown on magnesium are generally thin and porous, poorly adherent to the substrate and often need additional post-treatments [31,32]. Sealing method based on cerium and phosphate appears to be the most effective way to significantly improve the corrosion properties of PEO coatings on magnesium [33–35]. In addition, the PEO process is

* Corresponding author at: Université de Lorraine, CNRS, IJL, F-54000 Nancy, France.
E-mail address: julien.martin@univ-lorraine.fr (J. Martin).

https://doi.org/10.1016/j.surfcoat.2020.125756
Received 29 February 2020; Received in revised form 6 April 2020; Accepted 7 April 2020
Available online 08 April 2020

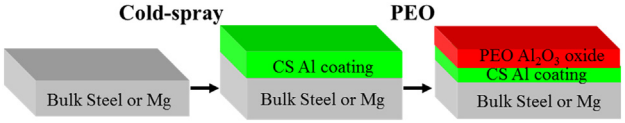

Fig. 1. Schematic description of the duplex surface treatments performed on S235 steel and EV31 magnesium substrates combining cold-spray (CS) and plasma electrolytic oxidation (PEO) processes.

Table 1
Elemental composition of the commercial EV31 magnesium substrate.

Elements	Nd	Gd	Zn	Zr	Mg
in wt%	2.60	1.38	0.25	0.66	Balance

Table 2
Elemental composition of the commercial S235 steel substrate.

Elements	Mn	C	Si	P	S	Fe
in wt%	1.4	0.17	0.05	0.035	0.035	Balance

Table 3
Elemental composition of the commercial 1050 aluminium used as substrate and as cold-sprayed powder.

Elements	Fe	Si	Zn	Cu, Mg, Mn, Ti	Al
in wt%	0.40	0.25	0.07	< 0.05	Balance

Table 4
Conditions of elaboration of the different samples using cold-spray (CS) and plasma electrolytic oxidation (PEO) processes.

Substrate	CS process (thickness of Al 1050)	PEO process (processing time)	Reference name
Al (1050)	0 µm	8 min	Al + CS0µm + PEO8min
Al (1050)	0 µm	20 min	Al + CS0µm + PEO20min
Al (1050)	0 µm	35 min	Al + CS0µm + PEO35min
Mg (EV31)	66 ± 15 µm	0 min	Mg + CS66µm + PEO0min
Mg (EV31)	66 ± 15 µm	8 min	Mg + CS66µm + PEO8min
Mg (EV31)	66 ± 15 µm	20 min	Mg + CS66µm + PEO20min
Mg (EV31)	66 ± 15 µm	35 min	Mg + CS66 µm + PEO35min
Mg (EV31)	220 ± 25 µm	0 min	Mg + CS220µm + PEO0min
Mg (EV31)	220 ± 25 µm	8 min	Mg + CS220µm + PEO8min
Mg (EV31)	220 ± 25 µm	20 min	Mg + CS220µm + PEO20min
Mg (EV31)	220 ± 25 µm	35 min	Mg + CS220µm + PEO35min
Steel (S235)	80 ± 15 µm	0 min	St + CS80µm + PEO0min
Steel (S235)	80 ± 15 µm	8 min	St + CS80µm + PEO8min
Steel (S235)	80 ± 15 µm	20 min	St + CS80µm + PEO20min
Steel (S235)	80 ± 15 µm	35 min	St + CS80µm + PEO35min
Steel (S235)	190 ± 25 µm	0 min	St + CS190µm + PEO0min
Steel (S235)	190 ± 25 µm	8 min	St + CS190 µm + PEO8min
Steel (S235)	190 ± 25 µm	20 min	St + CS190µm + PEO20min
Steel (S235)	190 ± 25 µm	35 min	St + CS190µm + PEO35min

Table 5
Parameters of the cold-spray (CS) process.

Parameters	Values
Sprayed powder	Commercial 1050 aluminium alloy
Powder shape	Spherical
Powder size	10 ± 3 µm
Carrier gas type	Nitrogen (N_2)
Gas pressure	2.4 MPa
Gas temperature	340 °C
Nozzle traverse speed	90 mm.s^{-1}
Nozzle stand-off distance	30 mm

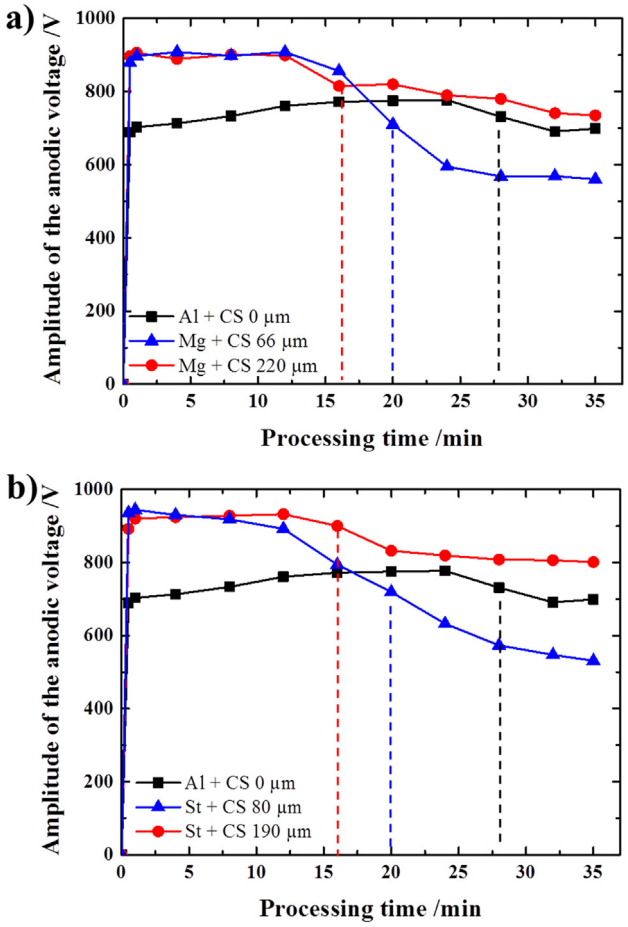

Fig. 2. Evolutions of the anodic voltage amplitude as a function of the PEO processing time **a)** for Al 1050 substrate (without cold-sprayed Al coating) and Mg substrates (with 66 and 220 µm cold-sprayed Al coatings) and **b)** for Al 1050 substrate (without cold-sprayed Al coating) and steel substrates (with 80 and 190 µm cold-sprayed Al coatings). Vertical dash lines indicate the PEO processing time at which the "soft" regime occurs. Reference name of each sample is given in Table 4.

strictly limited to aluminium, titanium, magnesium and zirconium alloys and it remains ineffective on other metals [5,6]. For example, it does not allow surface protection of ferrous metals for which electrodeposition of Zn- and Ni-based alloys are still widely used at the industrial scale. However, electrodeposition technologies use concentrated acids (*e.g.* boric acid) or alkaline electrolytes containing toxic cyanides compounds [36].

In this context, duplex treatments can address these issues and widen the use of the PEO process. In this paper, it is proposed to investigate the feasibility of a duplex surface treatment combining cold-spray deposition and PEO technology. Studies reporting on the combination of cold-spray and PEO are scarce in the literature, and to the knowledge of the authors, only two recently published works mentioned its use on an AZ91 magnesium alloy [37,38]. Although, improvements in the corrosion and wear resistance were observed, the effect of this duplex treatment on the growth mechanisms of the PEO coatings has not been considered as well as the feasibility to apply such duplex treatment on another magnesium alloy and also on a steel substrate.

2. Experimental procedure

As illustrated in Fig. 1, the process consists in first cold-spraying an aluminium coating on a metallic substrate that will be converted into

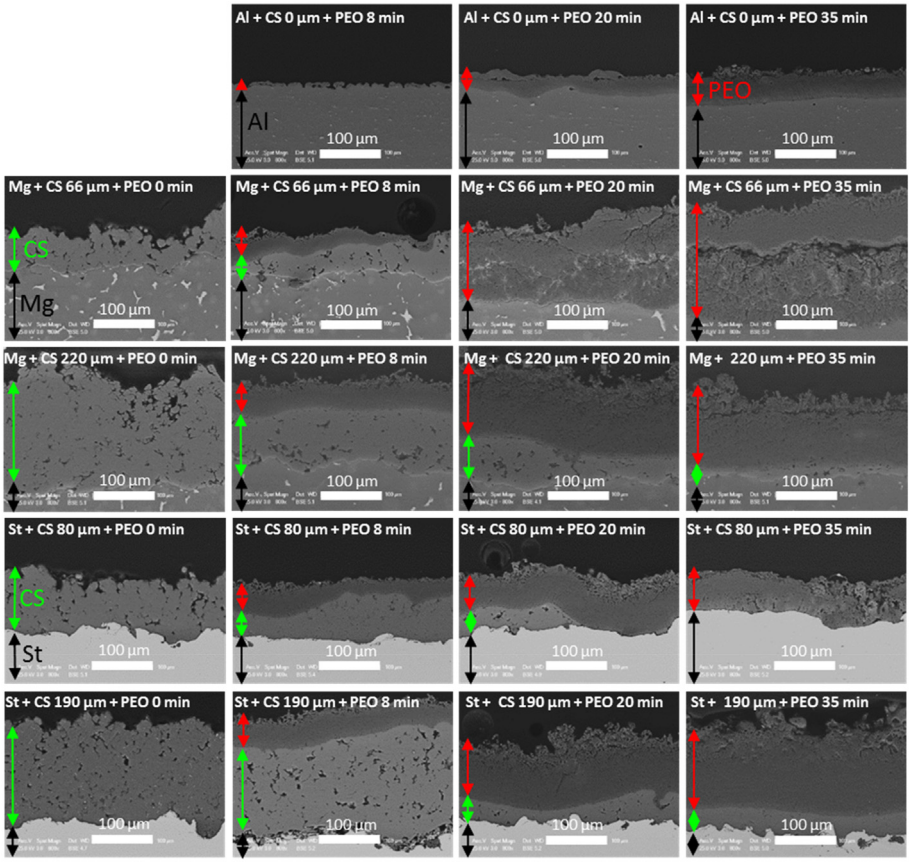

Fig. 3. Cross-section SEM micrographs of the cold-sprayed and PEO processed samples for different PEO processing time. Reference name of each sample is given in Table 4. Black arrows indicate the substrate (Al, Mg or Steel), green arrows indicate the cold-sprayed Al coating and red arrows indicate the PEO coating. (For interpretation of the references to colour in this figure legend, the reader is referred to the web version of this article.)

aluminium oxide by the use of the PEO process in a second step. For comparison reasons, bulk aluminium substrates were also processed using the same PEO conditions.

2.1. Materials

A commercial EV31 grade magnesium alloy and a commercial S235 steel were used as substrates. The chemical composition of Mg EV31 and S235 steel is given in Tables 1 and 2, respectively. All samples had a rectangular shape of 45 × 25 × 6 mm^3. Prior to be processed, the surface of the samples was shot blasted with corundum particles under 5 bars pressure. It allowed cleaning the surfaces (*e.g.* removal of organic contaminations or oxidation residues) as well as providing a sufficient roughness level to ensure adhesion of the aluminium sprayed coating. The resulting surface roughness R_a of the prepared samples was $R_a = 25 \pm 5$ µm and $R_a = 17 \pm 5$ µm for the magnesium and for the steel substrates, respectively. PEO coatings on pre-deposited aluminium were compared with PEO layers achieved on pure aluminium (Al 1050) bulk substrate using the same PEO conditions. The composition of Al 1050 grade material is given in Table 3. Table 4 summarizes the different samples that were processed for this study.

2.2. Cold-spray conditions

In the cold-spray (CS) process, also known as cold gas-dynamic spraying (CGDS), coatings are applied in the solid state by spraying metal powder at a high velocity on a substrate at greatly reduced temperatures compared to thermal spray techniques [39–41]. A schematic view of a typical cold-spray facility is presented in reference [40]. A carrier gas, usually nitrogen or helium, at pressure as high as 6 MPa and temperature ranging from 100 to 1100 °C, is expanded to supersonic speed through a converging-diverging De Laval nozzle. Particles are introduced in this gas flow at the inlet of the nozzle. Depending of the processing conditions applied, as well as on the morphology and the density of the sprayed particles, the metallic particles are accelerated through the nozzle at speeds exceeding 1600 $m{\cdot}s^{-1}$. The particles impact the substrate located approximately between 20 and 100 mm from the exit of the nozzle and form a more or less dense metal coating depending on the velocity of the particles. Thickness of the sprayed coating is also adjusted by repeated scans over the same area. Table 5 gives the main parameters of the cold-spray process that were used in the present study. The sprayed metallic powder consisted in a commercial 1050 grade aluminium for which the chemical composition is given in Table 3. Two different ranges of pre-coating thickness were prepared on both magnesium and steel substrates. For magnesium substrates, thicknesses of the aluminium layer deposited by cold-spray were 66 ± 15 µm and 220 ± 25 µm (see Table 4). For the steel substrate, thicknesses were 80 ± 15 µm and 190 ± 25 µm.

2.3. Plasma electrolytic oxidation conditions

A schematic view of a typical PEO treatment unit is presented in reference [5]. PEO treatments were run in a solution of potassium hydroxide ($[KOH] = 1\ g{\cdot}L^{-1} \cong 0.018\ mol{\cdot}L^{-1}$) and anhydrous sodium silicate ($[Na_2SiO_3] = 1.65\ g{\cdot}L^{-1} \cong 0.014\ mol{\cdot}L^{-1}$) diluted in deionised water. The measured pH and conductivity of the fresh electrolyte were 12.5 and 2.8 $mS{\cdot}cm^{-1}$, respectively. In order to limit the ageing effect of the electrolyte, a fresh electrolyte was renewed for each substrate. Two titanium plates 200 × 200 × 1 mm^3 in size were used as counter-electrodes. They were systematically located at 90 mm apart from the working electrode (Al1050, Mg EV31 and Steel S235). All the PEO treatments were performed using a pulsed bipolar current generator within the "soft" regime conditions [30]. The anodic to cathodic charge quantity ratio, $RCQ = Q_p/Q_n$, was set at a value of 0.9. The current pulse frequency (f) and the anodic current density (j_a) were set at 100 Hz and 48 $A{\cdot}dm^{-2}$ respectively. As reported in Table 4, the

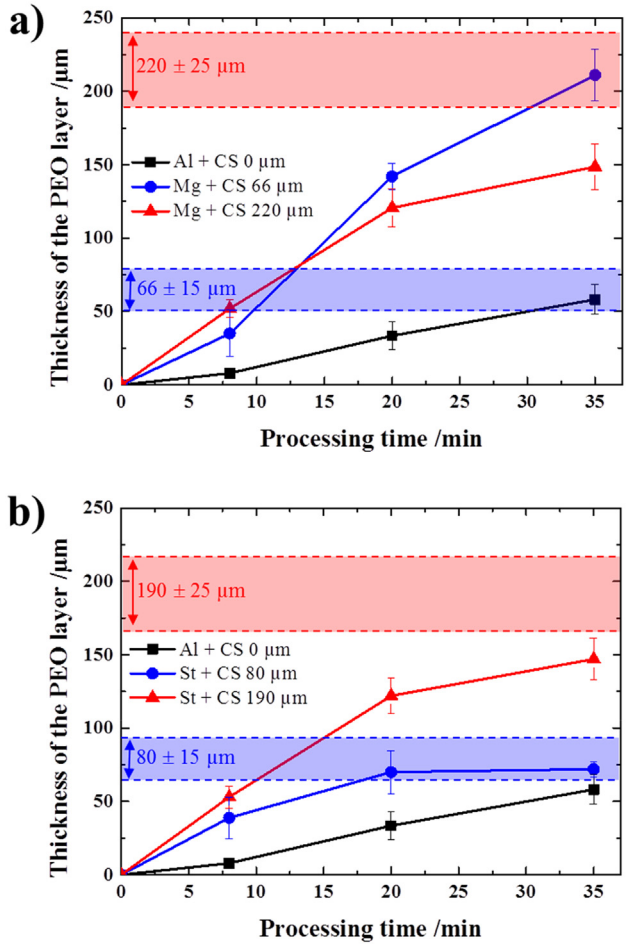

Fig. 4. Evolutions of the PEO oxide layer thickness as a function of the PEO processing time **a)** for Al 1050 and Mg substrates and **b)** for Al 1050 and steel substrates. Coloured boxes indicate thickness range of the different pre-deposit cold-sprayed Al coatings. Reference name of each sample is given in Table 4.

duration of the PEO treatments was set at 8, 20 and 35 min. After the PEO treatment, the processed sample was rinsed with ethanol, dried and stored in a dry environment before *ex-situ* characterization. The voltage-time response was recorded using a 1 GHz bandwidth oscilloscope (Agilent 54832B).

2.4. Ex-situ characterization of the coatings

Cross-sections of the treated samples were examined by SEM (FEG-SEM Philips XL 30S) working in backscattered electron mode (25 kV accelerating voltage). Prior to SEM observations, specimens with 5 × 5 × 6 mm^3 in size were cut, mounted in resin and finely polished with 1 µm diamond paste. SEM investigations were systematically done at the centre of the sample in order to avoid possible artefact due to edge effect. The coating thickness was determined as an average value of 10 measures taken on cross-section over 10 different positions (every 100 µm). Chemical composition and distribution of elements in the synthesized duplex coatings were determined by EDX analyses. The phase composition of the coatings was determined by X-ray diffraction (XRD) measurements in Bragg-Brentano geometry using the Cu-$K_{\alpha 1}$ radiation at $\lambda = 0.1542$ nm (Bruker D8 ADVANCE diffractometer). The step size and the scan range were set at 0.005° and from 20 to 90°, respectively. For XRD, specimens with 5 × 5 × 6 mm^3 in size were used. Finally, some X-ray micro-computed tomography (µCT) measurements were carried out to characterized porosities through the cold-sprayed aluminium coatings as well as through the PEO oxide layers. A Phoenix Nanotom X-ray µCT facility was used to characterize the morphology and the space distribution of pores in both the cold-sprayed and PEO coatings. Rectangular specimens with 2 × 2 × 2 mm^3 in size were characterized by µCT. The µCT procedure was based on the acquisition of a series of X-ray radiographs of a sample that rotated step by step around a vertical axis perpendicular to the incident X-ray beam. Images were recorded over a period of 6 s. A total of 1440 images were recorded for a scan duration of 144 min. A mathematical algorithm was used to reconstruct the internal 3D volume structure of the samples. The final resolution of the 3D-images was voxels of dimensions 1.5 × 1.5 × 1.5 μm^3. Below these dimensions, porosities were not detected.

3. Results

3.1. Establishment of the "soft" sparking regime

Fig. 2 shows the evolution of the anodic voltage amplitude as a function of the PEO processing time for the different duplex treatments summarized in Table 4. As previously reported, the "arc" to "soft" regime switching time is usually detected by the gradual drop in the anodic voltage amplitude during the PEO process [12,22,26]. The time at which "soft" regime occurs is usually determined at the inflexion point of the voltage curve. During the first minutes of treatment, *i.e.* in the "arc" sparking regime, Fig. 2 shows that the presence of a cold-sprayed aluminium coating on magnesium and steel substrates has a significant influence on the voltage amplitude compared to the reference PEO treatment performed on the bulk aluminium substrate. For instance, at $t = 5$ min, the anodic voltage amplitude is higher than 900 V for the duplex treatments while it is lower than 760 V for the reference PEO treatment performed on the bulk aluminium. Moreover, for this reference treatment, transition from the "arc" to the "soft" regime appears at about 28 min. In contrast, Fig. 2 evidences that all the duplex treatments performed on magnesium and steel substrates result in an earlier appearance of the "soft" sparking regime. This is particularly obvious for the thicker cold-sprayed aluminium coatings for which transition occurs before 18 min. For the thinner pre-deposited aluminium coatings, it is also apparent that the establishment of the "soft" regime is accompanied with a sharp drop in the anodic voltage amplitude (> 300 V).

3.2. Morphology and growth kinetic of the coatings

Fig. 3 shows the cross-sectional SEM micrographs of the PEO oxide layers grown within the different conditions as defined in Table 4. Cross-sectional views of the pre-deposited aluminium coatings on the magnesium and steel substrates are also presented in Fig. 3 (left-hand side column). The latter show that all the cold-sprayed aluminium coatings studied here are porous. For the bulk aluminium substrate, the cross-sectional SEM micrographs show the typical morphology of PEO coatings produced on aluminium alloys during the "arc" regime (at 8 and 20 min) and the "soft" regime (at 35 min). The pancake-like structure is the usual feature of PEO layers grown under the "arc" regime while a sponge-like structure known to incorporate elements from the electrolyte (*e.g.* Si, Na and K) is more developed over the top-surface under the "soft" regime. It is also apparent that with the transition from the "arc" to the "soft" sparking regime that occurs at about 28 min for the bulk aluminium substrate, the morphology gradually transforms into a more compact and a thicker oxide layer.

Interestingly, Fig. 3 clearly demonstrates the possibility to grow a PEO oxide layer through a cold-sprayed aluminium coating previously applied on magnesium and steel substrates. Whatever the nature of the metallic substrate (*i.e.* magnesium or steel), the thickness of the cold-sprayed aluminium coating and the PEO processing time, the duplex treatments result in thicker and more compact PEO oxide layers than those grown by PEO on pure aluminium substrate. Additionally, the

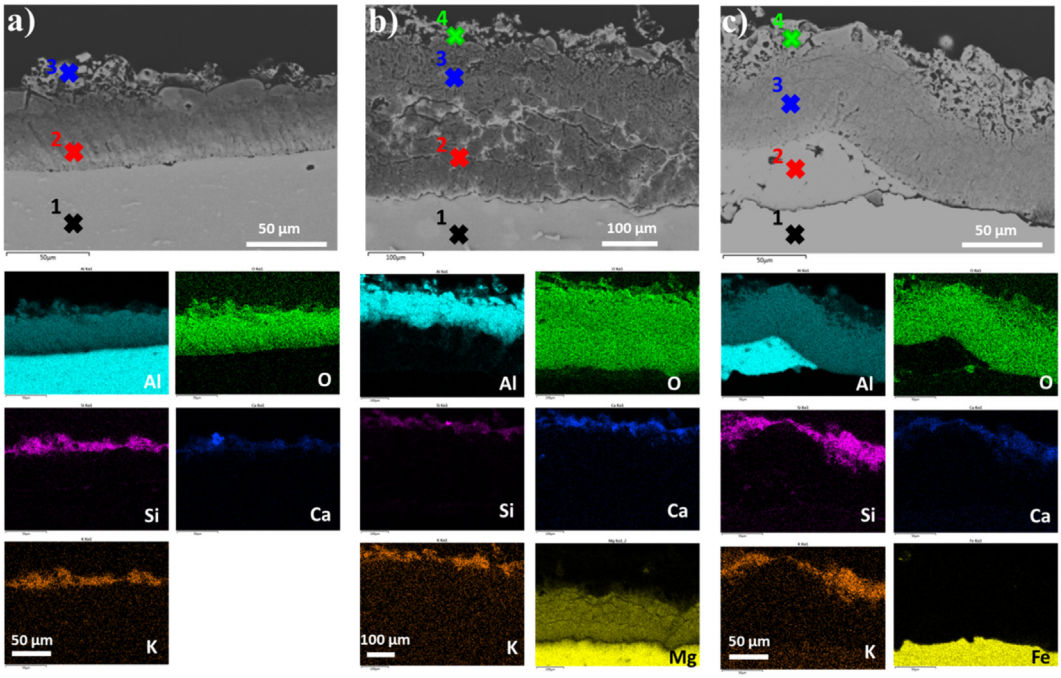

Fig. 5. Cross-sections SEM micrographs and the corresponding EDX element maps for the duplex coatings grown on **a)** bulk Al 1050 (Al + CS0µm + PEO35min), **b)** Mg EV31 (Mg + CS66µm + PEO20min) and **c)** S235 steel substrate (St + CS80µm + PEO20min). Coloured crosses indicate the localization of EDX measurements and element quantification given in Fig. 6 and Tables 6, 7 and 8.

top-surface of the PEO oxide layers grown for 20 min or more already exhibits the particular sponge-like structure achieved under the "soft" sparking regime. This agrees well with the voltage-time responses (Fig. 2) that show an earlier transition to the "soft" regime by using duplex treatments.

Concerning the cold-sprayed aluminium coatings < 80 µm in thickness, growth of the PEO oxide layers is different depending on the processed substrate. In the case of the magnesium substrate, after 20 min processing time, the thickness of the PEO oxide layer reaches and then exceeds the thickness of the pre-deposited aluminium coating (samples Mg + CS66µm + PEO20min and Mg + CS66µm + PEO35min in Fig. 3). This suggests that the magnesium substrate is PEO converted in magnesium oxide beyond the total conversion of the sprayed Al layer. This is particularly obvious at 35 min where signs of delamination can be observed exactly at the location of the former aluminium/magnesium interface. In contrast, for the steel substrate, the PEO oxide layer reaches the aluminium / steel interface at about 20 min after which growth of the oxide layer seems to stop (samples St + CS80µm + PEO20min and St + CS80µm + PEO35min in Fig. 3). Interestingly, after 35 min, no delamination is observed at the interface between the elaborated PEO coating and the steel substrate. This can be explained by the initial high level of roughness over the steel surface that ensures an efficient anchor of the coating.

Fig. 4 depicts the evolution of the average thickness of the overall PEO oxide layer with the processing time for the different treatments summarized in Table 4. Fig. 4 evidences an enhancement of the growth kinetic of the PEO oxide layer, by a factor 3 or more, when applying duplex treatments (~6 µm·min^{-1}) than using one-step PEO process (~1.5 µm·min^{-1}). For thinner cold-sprayed aluminium coatings (down to 80 µm in thickness), and as previously observed in Fig. 3, a difference in the growth kinetic is pointed out between the magnesium and the steel substrates. Indeed, for the magnesium substrate, the final thickness of the PEO oxide layer (215 ± 20 µm at 35 min) clearly exceeds the thickness of the sprayed aluminium coating (66 ± 15 µm). Thus, it confirms the fact that the magnesium substrate is PEO converted in magnesium oxide beyond the total conversion of the cold-spray deposited Al layer. Oppositely, for the steel substrate, once the sprayed aluminium coating is PEO converted, at about 20 min, growth of the PEO oxide layer stops. Finally, for the thicker cold-sprayed aluminium coatings (up to 190 µm in thickness), and whatever the processed substrate (Mg or steel), a slight decrease in the growth kinetic is observed after about 20 min (~4 µm·min^{-1}).

3.3. Chemical and crystallographic compositions of the coatings

Fig. 5 shows specific cross-sectional SEM views and the associated EDX elemental map distributions (Al, O, Si, Ca, K, Mg and Fe elements) throughout the coatings synthesized using a single 35 min PEO process on a bulk aluminium substrate (sample Al + CS0µm + PEO35min) and using the duplex treatments on magnesium and steel alloys (samples Mg + CS66µm + PEO20min and St + CS80µm + PEO20min). In complement, Fig. 6 shows EDX spectra recorded at different locations over the sample cross-sections (indicated by coloured crosses in Fig. 5). The corresponding quantifications in elements are given in Tables 6, 7 and 8. First of all, whatever the processed substrate (Al, Mg or steel), these element maps evidence an outer sponge-like structure that incorporates elements from the electrolyte *e.g.* O, Si, Ca and K. This is usually encountered for PEO treatments conducted on aluminium under the "soft" sparking regime. In addition, for the bulk aluminium substrate, Fig. 5a shows that the inner sublayer exclusively consists of Al and O (Table 6). For the magnesium substrate with a thin aluminium pre-coating (Mg + CS66µm + PEO20min), the synthesized PEO coatings consist of (i) a sponge-like outer sublayer enriched in Si, Ca and K, (ii) a denser intermediate sublayer rich in Al and O, and (iii) an inner sublayer rich in Mg and O close to the magnesium substrate (Fig. 5b). This inner sublayer exhibits cracks that mainly develop parallel to the metal/oxide interface. The element quantification performed in this inner sublayer clearly suggests the presence of a magnesium oxide and the absence of an aluminium oxide (Table 7). In the case of the steel substrate (St + CS80µm + PEO20min) (Fig. 5c), the PEO coating shows a thick sponge-like outer sublayer and a compact inner sublayer rich in Al and O (Table 8). It is also worth mentioning that the EDX measurements do not show the presence of oxidized iron even close to

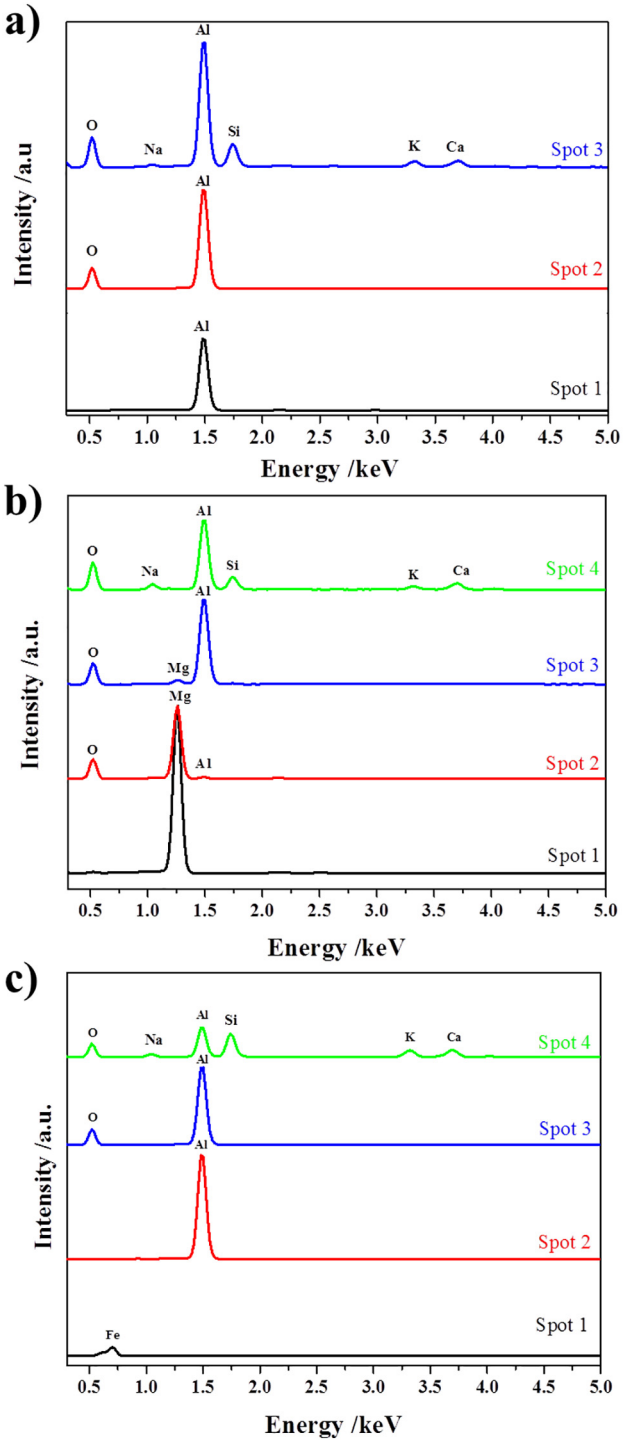

Fig. 6. EDX spectra recorded at different locations over the cross-section of the coatings grown on **a)** bulk Al 1050 (Al + CS0μm + PEO35min), **b)** Mg EV31 (Mg + CS66μm + PEO20min) and **c)** S235 steel substrate (St + CS80μm + PEO20min). Location of the different spots is defined in the SEM cross-section micrographs in Fig. 5.

the steel interface.

XRD analyses of the processed samples point out the presence of Al as well as crystalline α- and η-alumina peaks (Fig. 7). The Al peaks originate from the aluminium substrate or from the cold-sprayed aluminium coating. The presence of α- and η-alumina is usual for PEO oxide layers grown on aluminium. The transition from the "arc" to the "soft" sparking regime is known to be concomitant with an increase in the α-alumina proportion in the PEO layer. This is confirmed by the

Table 6
Elemental composition from EDX measurements performed at different locations over the cross-section of the processed Al1050 substrate (without cold-sprayed Al coating).

Elements	Al	O	Si	Ca	K	Na
Spot 1* (in wt%)	100	–	–	–	–	–
Spot 2 (in wt%)	57	43	–	–	–	–
Spot 3 (in wt%)	39	41	12	3	3	2

* Location of the different spots is defined in the SEM cross-section in Fig. 5a.

Table 7
Elemental composition from EDX measurements performed at different locations over the cross-section of the processed Mg EV31 substrate (with cold-sprayed Al coating).

Elements	Mg	Al	O	Si	Ca	K	Na
Spot 1* (in wt%)	100	–	–	–	–	–	–
Spot 2 (in wt%)	58	3	39	–	–	–	–
Spot 3 (in wt%)	2	54	44	–	–	–	–
Spot 4 (in wt%)	–	32	45	9	6	4	4

* Location of the different spots is defined in the SEM cross-section in Fig. 5b.

Table 8
Elemental composition from EDX measurements performed at different locations over the cross-section of the processed S235 steel substrate (with cold-sprayed Al coating).

Elements	Fe	Al	O	Si	Ca	K	Na
Spot 1* (in wt%)	100	–	–	–	–	–	–
Spot 2 (in wt%)	–	100	–	–	–	–	–
Spot 3 (in wt%)	–	56	44	–	–	–	–
Spot 4 (in wt%)	–	27	42	16	6	6	3

* Location of the different spots is defined in the SEM cross-section in Fig. 5c.

relative increase in the intensity of the α-alumina peaks with the processing time compared to the intensity of the η-alumina peaks. For the magnesium substrate with a pre-deposited aluminium coating (Fig. 7b), XRD patterns also show the presence of magnesium oxide (MgO) and forsterite (Mg_2SiO_4) peaks after 20 min processing time. It definitively confirms that the oxidation of the magnesium substrate takes place after the complete oxidation of the pre-deposited aluminium coating. Their low peak intensity is due to the fact that the MgO- and Mg_2SiO_4-containing sublayer is located beneath the thick aluminium oxide outer sublayer as observed in Fig. 5b. Interestingly, by using a duplex treatment involving cold-spray and PEO processes on a magnesium substrate, this result also demonstrates the possibility to produce a composite ceramic-based multilayer on a lightweight metal. Finally, for the steel substrate on which an aluminium pre-coating was sprayed, XRD patterns in Fig. 7c only show the presence of Al peaks as well as crystalline α- and η-alumina peaks. For longer PEO processing time, although growth of the PEO coating stops, the relative intensity of the α-alumina peaks seems to increase compared to the intensity of the η-alumina peaks. This suggests the gradual transformation of the η-alumina into α-alumina for longer PEO processing time. This point needs however further detailed investigations. In addition, Fig. 7c also confirms the absence of oxidized iron through the PEO coating.

4. Discussion

The discussion hereafter focuses on the influence of the porosity on the PEO process of aluminium. Particularly, a descriptive mechanism is proposed to explain the role played by the porosities through a pre-deposited aluminium coating on the subsequent growth of a PEO oxide layer. Indeed, results have shown that growth kinetic of PEO oxide layers is greatly enhanced (by a factor up to 3) when applied to cold-

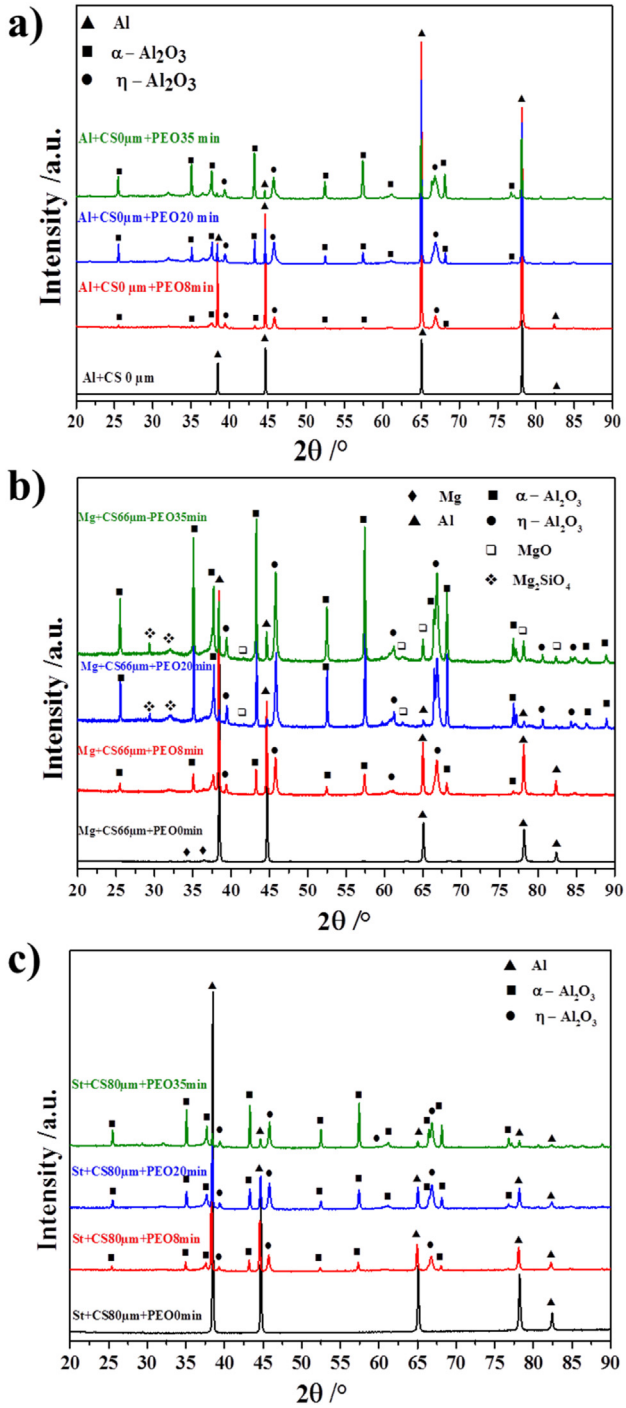

Fig. 7. XRD patterns (using Bragg-Brentano geometry) of the coatings synthesized using cold-spray and PEO treatments at different processing time (0, 8, 20 and 35 min) for **a)** Bulk Al 1050 substrate, **b)** Mg EV31 substrate and **c)** S235 steel substrate. Reference name of each sample is given in Table 4.

sprayed aluminium coatings compared with a bulk aluminium substrate. At the same time, results also show that the cold-sprayed aluminium coatings exhibit a high level of porosity throughout their thickness (see Fig. 3). This is particularly obvious in the cross-sectional SEM view of a steel substrate covered with a cold-sprayed aluminium coating (80 ± 15 μm in thickness) that was then shortly PEO processed (for 8 min processing time) (Fig. 8). Large and extended pores up to 50 μm in length are observed through the pre-deposited aluminium coating.

In complement to these SEM observations, X-ray micro-computed tomography (μCT) measurements were also carried out to characterize these porosities in both the cold-sprayed aluminium coatings and the grown PEO oxide layers. Fig. 9 shows the μCT visualizations of pores into the PEO coating elaborated on a cold-spray coated steel substrate (St + CS190μm + PEO35min). The associated schema in Fig. 9 allows localizing the μCT probed volume. The PEO outer sublayer consists in small numerous pores while the cold-sprayed aluminium coating exhibits fewer but larger pores. The size of pores into the PEO oxide layer is < 1.5 μm in length, which is the detection limit of the μCT equipment (< 3.38×10^{-9} mm^3 in volume). For the cold-sprayed coating, the length path of the detected porosities varies between 10s and 100 s of μm while the average volume ranges between 10^{-8} and 10^{-5} mm^3. Interestingly, and contrary to observations performed on cross-sectional SEM micrographs, the μCT visualizations in Fig. 9 evidence the presence of interconnected pores through the cold-sprayed aluminium coating forming a network of large porosities. At the beginning of the PEO process, when the sample is immersed into the electrolyte, it would be reasonable to expect that the presence of such open porosities allow the electrolyte to fill in the porosities and deeply penetrate into the cold-sprayed aluminium coating.

The EDX element maps in Fig. 8 confirm this statement since elements from the electrolyte, especially Si and O, are detected into the porosities of the pre-deposited aluminium coating. These elements are found far advanced from the front line of the aluminium oxidation. For these advanced sites, it suggests that conversion of aluminium into alumina has already started. This is confirmed in Fig. 10 where oxidized regions ahead from the PEO oxidation front line are observed. Interestingly, these oxidized regions clearly exhibit the same shape and size than the porosities detected by μCT through the cold-sprayed aluminium coatings.

Based on these observations, a growth mechanism of PEO coating in porous aluminium is schematically depicted in Fig. 11 and described hereafter. Before applying the current to the electrodes, the sample is immersed in the electrolyte. This electrolyte penetrates into the connected porosities of the cold-sprayed aluminium layer. When applying the current, and during the first seconds of treatment, the voltage increases rapidly due to the growth a thin insulating oxide layer over the processed surface. In the case of the sprayed coatings that exhibit open porosities, breakdown value appears at higher voltage than for the bulk aluminium substrate (see Fig. 2) due to higher specific surface. Indeed, accumulated charges throughout the insulating layer that are needed to reach the dielectric breakdown voltage remain higher with a higher specific surface. As the PEO process continues, the “arc” regime takes place first and arcs appear over the processed surface. Strong arcs ignite but, in the case of the sprayed aluminium coatings, they turn earlier into tiny or even not visible micro-discharges whose behaviour is comparable to the inner D-type micro-discharges appearing inside the PEO coating during the “soft” regime [2,12,30]. On this point, although the high level of porosity through the cold-sprayed aluminium coating seems to be responsible, it remains that further investigations are needed to better understand the earlier occurrence of the “soft” regime in the case of a duplex treatment (see Fig. 2). Once the “soft” regime is established, a sponge-like phase enriched in elements from the electrolyte grows at the top-surface of the PEO coatings. This can explain that, after just ten minutes of PEO treatment, a well-developed sponge-like structure is observed at the top surface of the duplex coating. In contrast, for the bulk aluminium, this sponge like structure grows later, after about 20 min (see Fig. 3). Inner micro-discharges that appear inside porosities of the pre-deposited aluminium coating gradually convert the surrounding aluminium into alumina. Thus, the growth front of the PEO oxide layer extends not only vertically as observed for the bulk aluminium but also laterally. As the process progresses, the porosities are gradually filled with aluminium oxide trapping elements from the electrolyte inside the inner dense PEO oxide sublayer. This explains the presence of such elements, mainly Si, throughout the overall PEO coatings (see Fig. 8). In contrast, for the PEO process of the

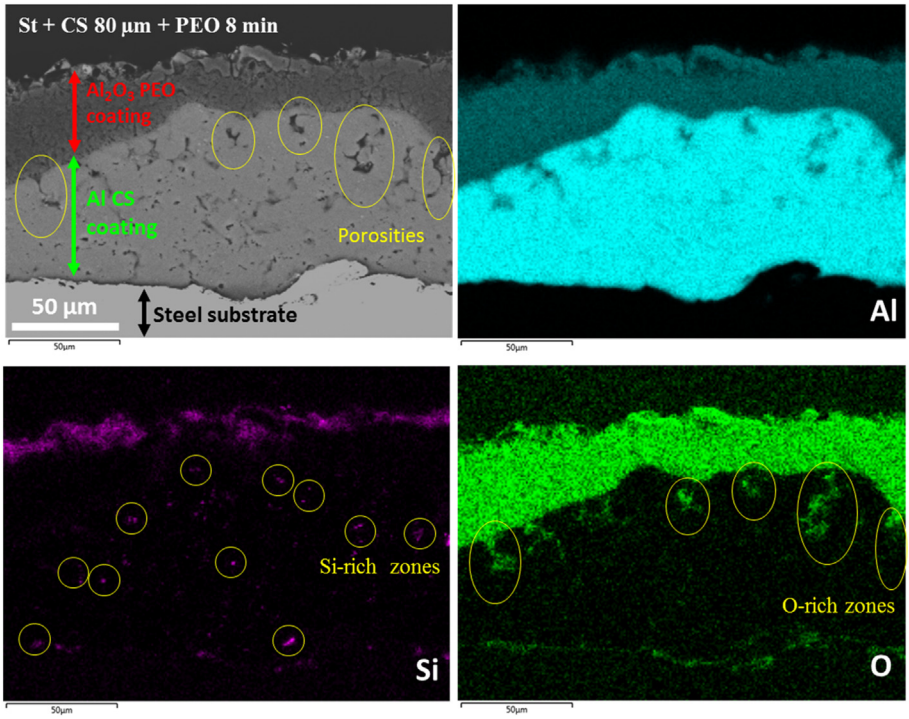

Fig. 8. Cross-sections SEM micrographs and corresponding EDX element maps (Al, Si and O) of a PEO coating grown on a pre-deposited steel substrate (St + CS80µm + PEO8min).

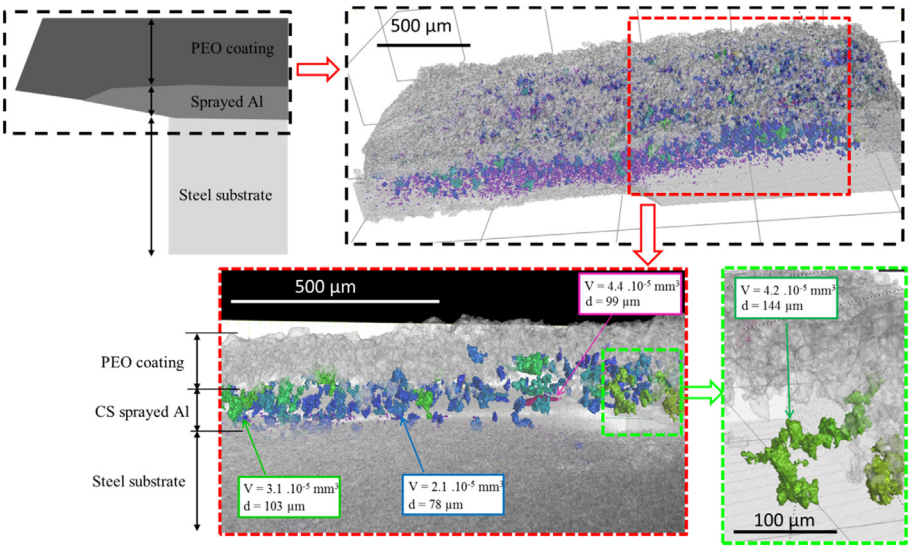

Fig. 9. X-ray micro-tomography images of a PEO coating grown on a steel substrate (St + CS190µm + PEO35min). V is the volume of porosities. d is the path length of the porosities.

bulk aluminium, the inner oxide sublayer is depleted in such elements. Finally, for the duplex treatments, the oxidized areas that consist in advanced fronts of oxidation overlap with the adjacent ones forming a thicker PEO coating compared to those observed for the PEO process of bulk aluminium.

5. Conclusions

The feasibility of duplex surface treatments involving cold-spray (CS) and plasma electrolytic oxidation (PEO) techniques was investigated. For this purpose, cold-sprayed aluminium coatings with various thicknesses were pre-deposited on magnesium and steel substrates and they were then PEO processed during various processing time. Results clearly demonstrate the possibility to grow an alumina PEO coating on magnesium and steel substrates cold-sprayed with porous aluminium. Compared to conventional PEO treatments performed on bulk aluminium substrates, growth kinetic of the PEO oxide layer is greatly enhanced by using a duplex treatment. While porosities in the cold-sprayed coatings are generally undesired, they seem here to have a very positive effect on the PEO growth kinetics. A descriptive growth mechanism was proposed. Such a duplex treatment offers new opportunities to protect surface of magnesium alloys and ferrous metals for which direct PEO process remains tricky and even not possible. Further investigations are now needed to study the properties of such duplex coatings such as wear resistance and corrosion resistance.

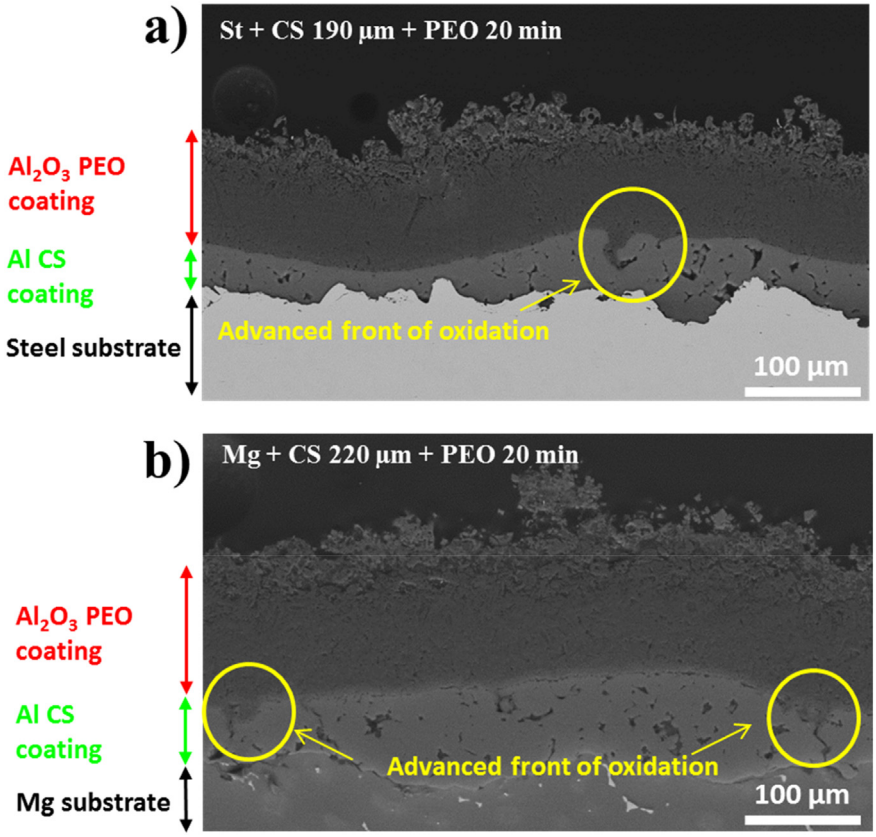

Fig. 10. Cross-section SEM micrographs of the cold-sprayed and PEO processed samples (for 20 min) for **a)** a steel substrate with 190 µm cold sprayed Al coating and **b)** a Mg substrate with 220 µm cold-sprayed Al coating. Yellow rings indicate advanced fronts of the oxidation. (For interpretation of the references to colour in this figure legend, the reader is referred to the web version of this article.)

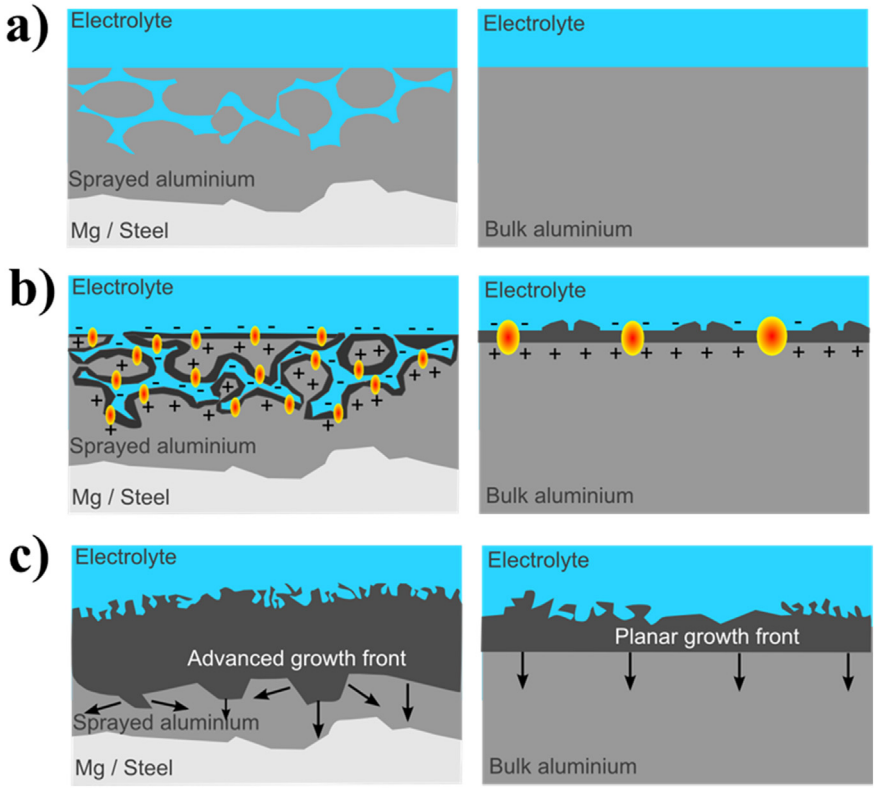

Fig. 11. Schematics of the influence of the porosities inside a cold-sprayed aluminium coating on the growth of a PEO oxide layer, **a)** before applying the current to the electrodes, **b)** during the first minutes of the PEO process and **c)** after longer PEO processing time.

CRediT authorship contribution statement

J. Martin:Conceptualization, Methodology, Investigation, Formal analysis, Writing - original draft, Supervision, Writing - review & editing.**K. Akoda**:Investigation, Formal analysis, Writing - review & editing.**V. Ntomprougkidis**:Methodology, Writing - original draft, Writing - review & editing.**O. Ferry**:Formal analysis, Writing - review & editing.**A. Maizeray**:Writing - original draft, Writing - review & editing.**A. Bastien**:Formal analysis, Writing - review & editing.**P. Brenot**:Conceptualization, Supervision, Writing - review & editing.**G. Ezo'o**:Conceptualization, Supervision, Writing - review & editing.**G. Henrion**:Conceptualization, Methodology, Supervision, Writing - review & editing.

Declaration of competing interest

The authors declare no competing financial interests.

Acknowledgments

- This work was supported by the French Government through the programme "Investissements d'avenir" operated by the French National Research Agency (ANR) and referenced to as ANR-11-LABX-0008-01 ('LabEx DAMAS').
- This work was also partly supported by ICÉEL Carnot Institute through the project "SOPRODSYSE"
- The authors would like to acknowledge contributions of the following:

– Mr. P. Boulet and the competence cluster on X-ray diffraction (CC-Xγ) at Institut Jean Lamour for providing advices in XRD measurements and analyses.
– Mrs. S. Mathieu and the competence cluster on electron microscopy (CC 3 M) at Institut Jean Lamour for providing advices in SEM observations and EDX analyses.

Data availability

The data that support the findings of this study are available from the corresponding author,
J. Martin, upon reasonable request.

Authorship statement

The submission of the manuscript has been approved by all co-authors.

References

[1] Gh. Barati Darband, M. Aliofkhazraei, P. Hamghalam, N. Valizade, Plasma electrolytic oxidation of magnesium and its alloys: mechanism, properties and applications, J. Magnesium Alloy. 5 (2017) 74–132.
[2] Y.L. Cheng, J. Cao, M. Mao, H. Xie, P. Skeldon, Key factors determining the development of two morphologies of plasma electrolytic coatings on an Al-Cu-Li alloy in aluminate electrolytes, Surf. Coat. Technol. 291 (2016) 239–249.
[3] Y.L. Cheng, J. Cao, Z. Peng, Q. Wang, E. Matykina, P. Skeldon, G.E. Thompson, Wear resistant coatings formed on Zircaloy-2 by plasma electrolytic oxidation in sodium aluminate electrolytes, Electrochim. Acta 116 (2014) 453–466.
[4] A. Mathis, E. Rocca, D. Veys-Renaux, J. Tardelli, Electrochemical behaviour of titanium in KOH at high potential, Electrochim. Acta 202 (2016) 253–261.
[5] A.L. Yerokhin, X. Nie, A. Leyland, A. Matthews, S.J. Dowey, Plasma electrolysis for surface engineering, Surf. Coat. Technol. 122 (1999) 73–93.
[6] P. Gupta, G. Tenhundfeld, E.O. Daigle, D. Ryabkov, Electrolytic plasma technology: science and engineering - an overview, Surf. Coat. Technol. 201 (2007) 8746–8760.
[7] J.A. Curran, T.W. Clyne, Thermo-physical properties of plasma electrolytic oxide coatings on aluminium, Surf. Coat. Technol. 199 (2005) 168–176.
[8] J.A. Curran, H. Kalkanci, Y. Magurova, T.W. Clyne, Mullite-rich plasma electrolytic oxide caotings for thermal barrier applications, Surf. Coat. Technol. 201 (2007) 8683–8687.
[9] E. Matykina, A. Berkani, P. Skeldon, G.E. Thompson, Real-time imaging of coating growth during plasma electrolytic oxidation of titanium, Electrochim. Acta 53 (2007) 1987–1994.
[10] F. Monfort, A. Berkani, E. Matykina, P. Skeldon, G.E. Thompson, H. Habazaki, K. Shimizu, Development of anodic coatings on aluminium under sparking conditions in silicate electrolyte, Corros. Sci. 49 (2007) 672–693.
[11] V. Dehnavi, X.Y. Liu, B.L. Luan, D.W. Shoesmith, S. Rohani, Phase transformation in plasma electrolytic oxidation on 6061 aluminium alloy, Surf. Coat. Technol. 251 (2014) 106–114.
[12] J. Martin, A. Nominé, V. Ntomprougkidis, S. Migot, S. Bruyère, F. Soldera, T. Belmonte, G. Henrion, Formation of a mestastable nanostructured mullite during plasma electrolytic oxidation of aluminium in "soft" regime condition, Mater. Design 180 (2019) 107977.
[13] A.L. Yerokhin, L.O. Snizhko, N.L. Gurevina, A. Leyland, A. Pilkington, A. Matthews, Discharge characterization in plasma electrolytic oxidation of aluminium, J. Phys. D. Appl. Phys. 36 (2003) 2110–2120.
[14] R.O. Hussein, X. Nie, D.O. Northwood, A. Yerokhin, A. Matthews, Spectroscopic study of electrolytic plasma and discharging behaviour during the plasma electrolytic oxidation (PEO) process, J. Phys. D. Appl. Phys. 43 (2010) 105203.
[15] J. Jovović, S. Stojadinović, N.M. Šišović, N. Konjević, Spectroscopic study of plasma during electrolytic oxidation of magnesium- and aluminium-alloy, J. Quant. Spectrosc. Rad. Trans. 113 (2012) 1928–1937.
[16] S. Stojadinović, J. Jovović, M. Petković, R. Vasilić, N. Konjević, Investigation of plasma electrolytic oxidation on valve metals by means of molecular spectroscopy – a review, RSC Adv. 4 (2014) 25759–25789.
[17] T.W. Clyne, S.C. Troughton, A review of recent work on discharge characteristics during plasma electrolytic oxidation of various metals, Int. Mater. Rev. 64 (2019) 127–162.
[18] F. Simchen, M. Sieber, T. Lampke, Electrolyte influence on ignition of plasma electrolytic oxidation processes on light metals, Surf. Coat. Technol. 315 (2017) 205–213.
[19] E. Matykina, R. Arrabal, F. Monfort, P. Skeldon, G.E. Thompson, Incorporation of zirconia into coatings formed by DC plasma electrolytic oxidation of aluminium in nanoparticle suspensions, Appl. Surf. Sci. 255 (2008) 2830–2839.
[20] X. Lu, M. Mohedano, C. Blawert, E. Matykina, R. Arrabal, K.U. Kainer, M.L. Zheludkevich, Plasma electrolytic oxidation coatings with particle additions – a review, Surf. Coat. Technol. 307 (2016) 1165–1182.
[21] B.S. Lou, Y.Y. Lin, C.M. Tseng, Y.C. Lu, J.G. Duh, J.W. Lee, Plasma electrolytic oxidation coatings on AZ31 magnesium alloys with Si3N4 nanoparticles additives, Surf. Coat. Technol. 332 (2017) 358–367.
[22] X. Tu, C. Miao, Y. Zhang, Y. Xu, J. Li, Plasma electrolytic oxidation of magnesium alloy AZ31B in electrolyte containing Al2O3 sol as additives, Materials 11 (2018) 1618–1629.
[23] J. Martin, A. Melhem, I. Shchedrina, T. Duchanoy, A. Nominé, G. Henrion, T. Czerwiec, T. Belmonte, Effects of electrical parameters on plasma electrolytic oxidation of aluminium, Surf. Coat. Technol. 221 (2013) 70–76.
[24] V. Dehnavi, B.L. Luan, D.W. Shoesmith, X.Y. Liu, S. Rohani, Effect of duty cycle and applied current frequency on plasma electrolytic oxidation (PEO) coating growth behaviour, Surf. Coat. Technol. 226 (2013) 100–107.
[25] V. Dehnavi, B.L. Luan, X.Y. Liu, D.W. Shoesmith, S. Rohani, Correlation between plasma electrolytic oxidation treatment stages and coating microstructure on aluminium under unipolar pulsed DC mode, Surf. Coat. Technol. 269 (2015) 91–99.
[26] V. Ntomprougkidis, J. Martin, A. Nominé, G. Henrion, Sequential run of the PEO process with various pulsed bipolar current waveforms, Surf. Coat. Technol. 374 (2019) 713–724.
[27] F. Jaspard-Mecuson, T. Czerwiec, G. Henrion, T. Belmonte, L. Dujardin, A. Viola, J. Beauvir, Tailored aluminium oxide layers by bipolar current adjustment in the Plasma Electrolytic Oxidation (PEO) process, Surf. Coat. Technol. 201 (2007) 8677–8682.
[28] A.B. Rogov, A. Yerokhin, A. Matthews, The role of cathodic current in plasma electrolytic oxidation of aluminium: phenomenological concepts of the "soft sparking" mode, Langmuir 33 (2017) 11059–11069.
[29] D.S. Tsai, G.W. Chen, C.C. Chou, Probe the micro arc softening phenomenon with pulse transient analysis in plasma electrolytic oxidation, Surf. Coat. Technol. 357 (2019) 235–243.
[30] J. Martin, A. Nominé, F. Brochard, J.L. Briançon, C. Noël, T. Belmonte, T. Czerwiec, G. Henrion, Delay in micro-discharges appearance during PEO of Al: evidence of a mechanism of charge accumulation at the electrolyte /oxide interface, Appl. Surf. Sci. 410 (2017) 29–41.
[31] J. Dou, Y. Chen, H. Yu, C. Chen, Research status, of magnesium alloys by micro-arc oxidation : a review, Surf. Eng. 33 (2017) 731–738.
[32] M. Toorani, M. Aliofkhazraei, Review of electrochemical properties of hybrid coating systems on Mg with plasma electrolytic oxidation process as pretreatment, Surf. Interface 14 (2019) 262–295.
[33] U. Malayoglu, K.C. Tekin, S. Shrestha, Influence of post-treatment on the corrosion resistance of PEO coated AM50B and AM60B Mg alloys, Surf. Coat. Technol. 205 (2010) 1793–1798.
[34] M. Sun, A. Matthews, A. Yerokhin, Plasma electrolytic oxidation coatings on cp-Mg with cerium nitrate and benzotriazole immersion post-treatments, Surf. Coat. Technol. 344 (2018) 330–341.
[35] M. Mohedano, C. Blawert, M.L. Zheludkevich, Cerium-based sealing of PEO coated AM50 magnesium alloy, Surf. Coat. Technol. 269 (2015) 145–154.
[36] M. Paunovic, M. Schlesinger, Fundamentals of Electro-Chemical Deposition, Wiley, New-York, 1998.
[37] L. Rama Krishna, G. Poshal, A. Jyothirmayi, G. Sundararajan, Compositionaly modulated CGDS + MAO duplex coatings for corrosion protection of AZ91 magnesium alloy, J. Alloys Comp. 578 (2013) 355–361.
[38] O. Tazegul, F. Muhaffel, O. Meydanoglu, M. Baydogan, E. Sabri Kayali, H. Cimenoglu, Wear and corrosion characteristics of novel alumina coatings

produced by micro arc oxidation on AZ91D magnesium alloy, Surf. Coat. Technol. 258 (2014) 168–173.
[39] V. Champagne, D. Helfritch, The unique abilities of cold spray deposition, Int. Mater. Rev. 61 (2016) 437–455.
[40] A. Moridi, S.M. Hassani-Gangaraj, M. Guagliano, M. Dao, Cold spray coating : review of material systems and future perspectives, Surf. Eng. 30 (2014) 369–395.
[41] M.R. Rokni, S.R. Nutt, C.A. Widener, V.K. Champagne, R.H. Hrabe, Review of relationship between particle deformation coating microstructure, and properties in high pressure cold spray, J. Therm. Spray Technol. 26 (2017) 1308–1355.